

Special Issue “Materiais 2015”

Shear fracture toughness and cohesive laws of adhesively-bonded joints

J.C.S. Azevedo^a, R.D.S.G. Campilho^a, F.J.G. Silva^{a,*}

^a*Departamento de Engenharia Mecânica, Instituto Superior de Engenharia do Porto, Instituto Politécnico do Porto,
Rua Dr. António Bernardino de Almeida, 431, 4200-072 Porto, Portugal*

Abstract

Adhesive bonding is a viable technique to reduce weight and complexity in structures. Additionally, this joining technique is also a common repair method for metal and composite structures. However, a generalized lack of confidence in the fatigue and long-term behaviour of bonded joints hinder their wider application. Suitable strength prediction techniques must be available for the application of adhesive bonding, and these can be based on mechanics of materials, conventional fracture mechanics or damage mechanics. These two last methodologies require the knowledge of the fracture toughness (G_C) of materials. Being damage mechanics-based, Cohesive Zone Modelling (CZM) analyses coupled with Finite Elements (FE) are under investigation. In this work, CZM laws were estimated in shear for a brittle adhesive (Araldite® AV138) and high-strength aluminium adherends, considering the End-Notched Flexure (ENF) test geometry. The CZM laws were obtained by an inverse methodology based on curve fitting, which made possible the precise estimation of the adhesive joints' behaviour. It was concluded that a unique set of shear fracture toughness (G_{IIC}) and shear cohesive strength (t_s^0) exists for each specimen that accurately reproduces the adhesive layer behaviour. With this information, the accurate strength prediction of adhesive joints in shear is made possible by CZM.

© 2017 Portuguese Society of Materials (SPM). Published by Elsevier España, S.L.U. All rights reserved.

Keywords: Crack growth; finite element analysis; fracture mechanics; structural integrity.

1. Introduction

The adhesive bonding technique enables a weight and complexity reduction in structures that require some joining technique to be used on account of fabrication/component shape issues. This compares to the large weight penalty of bolted or fastened joints, which adds to the requirement of dealing with the large stress concentrations around the structure' holes. However, some uncertainties regarding the fatigue and long-term behaviour of bonded joints still prevent adhesive bonding to be applied at a larger scale [1]. The availability of strength prediction techniques for adhesive joints is thus essential for their generalized application and it can rely on mechanics of materials,

conventional fracture mechanics or damage mechanics. These two last techniques require the measurement of the value of G_C of materials.

When dealing with real joints, mixed-mode behaviours are present, and the typical modelling approach is to define tensile and shear laws that can be combined by suitable criteria. Under shear, the ENF test is the most popular because of the specimen simplicity, easy test set-up and availability of accurate and straight-forward data reduction methods for estimation of G_{IIC} [2]. Since the introduction of this method by Barrett and Foschi [3], many works dealt with G_{IIC} determination for wood, composites and bonded joints, addressing effects such as test set-up and geometric parameters [4]. Data reduction techniques that account for large plasticization of modern toughened adhesives are available by advanced techniques and also the J -integral [5], this

* Corresponding author.

E-mail address: fgs@isep.ipp.pt (Francisco J.G. Silva)

last method additionally enabling the cohesive law estimation.

Within the framework of damage mechanics, a valid option is the use of CZM coupled with FE analyses. CZM applied to bonded joint prediction takes advantage of damage laws to simulate the behaviour of the adhesive, and eventually internal failures in the composite adherends (if applicable). CZM is based on the definition of the cohesive strength in tension and shear, t_n^0 and t_s^0 , respectively (relating to the end of the elastic regime and beginning of damage), and tensile fracture toughness (G_{IC}) and G_{IIC} (accounting for the amount of allowable plasticization prior to failure) [6]. Mainly three techniques can be used to estimate these properties: the property identification, inverse and direct methods. All of these depend on Double-Cantilever Beam (DCB), ENF or single-lap tests [7]. The property identification method lies on the separated calculation of the CZM parameters by proper tests, whilst inverse methods rely on estimating the CZM parameters by iterative fitting FE with experimental data (typically the load-displacement or P - δ curve) until reaching a good agreement between both. The direct method estimates the CZM law of a specific material or interface from the experimental data of fracture tests such as the DCB or ENF [8,9]. With this purpose, the test protocol usually requires measurement of additional parameters, such as the normal or shear opening at the crack tip. Carlberger and Stigh [10] studied, by the direct method, the mode I and mode II cohesive behaviour of adhesive layers of the epoxy Dow Betamate® XW1044-3 as a function of the adhesive thickness (t_A). The ENF testing protocol for mode II characterization relied on using a Linear Variable Differential Transformer (LVDT) mounted between rigid supports, one fixed to each adherend, to provide the real-time measurement of the shear relative displacement (δ_s). G_{IIC} showed to be more influent than t_s^0 by varying the value of t_A . However, the G_{IIC} dependency with t_A was much smaller than G_{IC} , although revealing an increasing trend with t_A . Alfredsson *et al.* [11] recently adapted the direct method in shear mode for thick adhesive layers, by considering a novel mathematical expression to estimate G_{IIC} . FE results showed that the pre-fracture behaviour is accurately captured.

Other works addressed the inverse technique. In a previous work [12], the shear CZM law of a ductile adhesive layer was estimated by the ENF test. The procedure involved the definition of G_{IIC} by suitable data reduction methods. The values of G_{IIC} were input in numerical models involving a trapezoidal CZM law

that accounted for the adhesive ductility. An inverse method, by fitting between the numerical and experimental P - δ curves, enabled finding t_s^0 and building the complete CZM law that reproduced the adhesive layer in shear. In the work of Chen *et al.* [13], an inverse technique was applied to determine the shear cohesive law of 2024-T3 aluminium alloy, considering the Arcan test geometry and different mode ratios, ranging from tensile to shear. A triangular CZM law was employed in the simulations. The inverse technique was based on minimizing the difference between experimental measurements on the load-extension curve and the respective numerical predictions.

In this work, CZM laws for adhesive joints considering a brittle adhesive were estimated. The ENF test geometry was selected based on overall test simplicity and results accuracy. The adhesive Araldite® AV138 was studied between high-strength aluminium adherends. Estimation of the CZM laws was carried out by an inverse methodology based on a curve fitting procedure.

2. Experimental Part

2.1. Adherend and adhesive materials

The adherends are made of a high-strength aluminium alloy (AA6082 T651). The mechanical properties of this material are available in the literature [14]. The adhesive Araldite® AV138 was previously characterized regarding the mechanical and toughness properties [14,15]. The collected data of the adhesive are summarized in Table 1.

Table 1. Properties of the adhesive Araldite® AV138 [14,15].

Property	AV138
Young's modulus, E (GPa)	4.89±0.81
Poisson's ratio, ν	0.35 ^a
Tensile yield strength, σ_y (MPa)	36.49±2.47
Tensile failure strength, σ_f (MPa)	39.45±3.18
Tensile failure strain, ϵ_f (%)	1.21±0.10
Shear modulus, G (GPa)	1.56±0.01
Shear yield strength, τ_y (MPa)	25.1±0.33
Shear failure strength, τ_f (MPa)	30.2±0.40
Shear failure strain, γ_f (%)	7.8±0.7
Toughness in tension, G_{IC} (N/mm)	0.20 ^b
Toughness in shear, G_{IIC} (N/mm)	0.38 ^b

^a manufacturer's data

^b estimated in reference [14]

2.2. Geometry and testing details

Fig. 1 depicts the geometry of the ENF specimens. The dimensions of the specimens are: mid-span $L_H=100$ mm, initial crack length $a_0\approx 60$ mm, $t_p=3$ mm, width $b=25$ mm and $t_A=1$ mm. The bonding faces were prepared by grit blasting, acetone cleaning and the specimens were assembled in a steel mould. To obtain a constant value of t_A , calibrated steel spacers were inserted between the adherends. Moreover, at the crack tip, a sharp pre-crack was induced by a 0.1 mm thick razor blade between the calibrated steel spacers. Curing was performed at room temperature. Preparation for testing consisted on removing the steel spacers, spraying the adherends' sides with brittle white paint to enable a clear identification of the crack length (a), and gluing a numbered scale in both adherends to aid the a measurement [16].

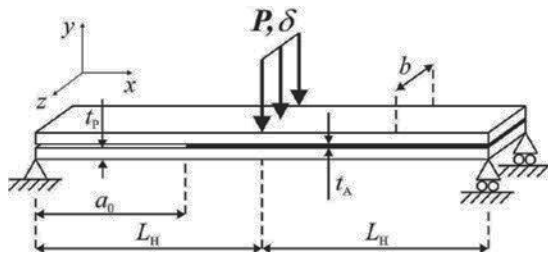


Fig. 1. Geometry and relevant dimensions of the ENF specimens.

Testing of the eight specimens was conducted in a Shimadzu AG-X 100 electro-mechanical testing machine equipped with a 100 kN load cell. Images were captured during the tests using an 18 MPixel digital camera, which enabled obtaining the values of a with accuracy.

2.3. Estimation of G_{IIC}

The evaluation of G_{IIC} carried out experimentally in this work was performed by four methods: the Compliance Calibration Method (CCM), the Direct Beam Theory (DBT), the Corrected Beam Theory (CBT) and the Compliance-Based Beam Method (CBBM). The CCM, DBT and CBT are widely described in the literature [12]. The CBBM enables the estimation of G_{IIC} only using the experimental compliance [17]. This technique relies on an equivalent crack that does not require measurement and is computed based on the current specimen's compliance [5]. This equivalent crack length (a_{eq}) accounts for the Fracture Process Zone (FPZ) effects at the crack tip (not taken into account when the real

crack length is considered). Detailed explanations of the method can be found in reference [17].

3. Numerical Part

3.1. Numerical considerations

A numerical FE analysis was carried out in Abaqus® aiming to obtain a shear cohesive law that is representative of the adhesive behaviour. The analysis is geometrically non-linear. Fig. 2 shows the applied boundary and loading conditions on the meshed model of an ENF joint. The FE mesh was built considering plane-strain four-node quadrilateral solid finite elements (CPE4 from Abaqus®) for the adherends, while the adhesive layer was modelled with four-node cohesive elements (COH2D4 from Abaqus®), including a bilinear (triangular) CZM.

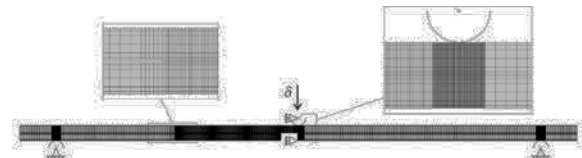


Fig. 2. Applied boundary and loading conditions on the meshed model of an ENF joint.

Wherever necessary, the mesh was constructed using bias effects to grade element size towards the more stress gradient regions. The boundary conditions consisted in fixing the supporting cylinders in the xy plane and restraining the loading cylinder in the horizontal direction. Additionally, the model was restrained in a discrete point in the horizontal direction to avoid undesired movement.

The numerical models were built individually for each specimen considering their particular dimensions, namely a_0 . The shear CZM law was input considering the obtained value of G_{IIC} for each specimen by the CBBM, based on previous evidence of best accuracy, comparing with the other 3 methods [12], and a typical t_s^0 value for the respective adhesive. From this point, a manual iterative procedure was undertaken by varying t_s^0 until a good accuracy between the experimental and numerical P - δ curves is attained, thus defining the final values of t_s^0 for each specimen.

3.2. Triangular CZM law

CZM are based on a relationship between stresses and relative displacements connecting homologous nodes of the cohesive elements (Fig. 3) to simulate the elastic behaviour up to a peak load and subsequent

softening [18,19]. The traction-separation law assumes an initial linear elastic behaviour followed by linear evolution of damage. The areas under the traction-separation laws in each mode of loading (tension and shear) are equalled to the respective value of G_C . Under mixed mode, energetic criteria are often used to combine tension and shear [20]. The quadratic nominal stress criterion is typically used for the initiation of damage. Complete separation can be predicted by a linear power law form of the required energies for failure in the pure modes. However, the mixed-mode behaviour is not particularly relevant for the shear analysis presented in this paper. For full details of the presented model, the reader can refer to reference [14].

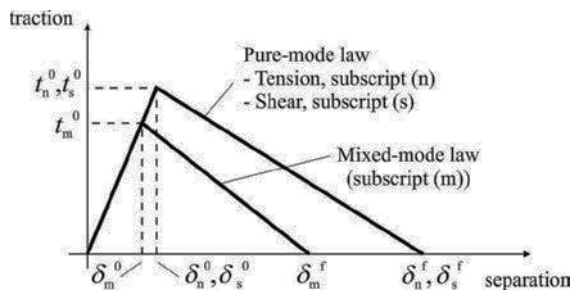


Fig. 3. Traction-separation law with linear softening law available in ABAQUS®.

4. Results

4.1. Estimation of G_{IIC}

Fig. 4 represents the experimental R -curves (plot of the shear strain energy release rate, G_{II} vs. a , for one representative tested specimen.

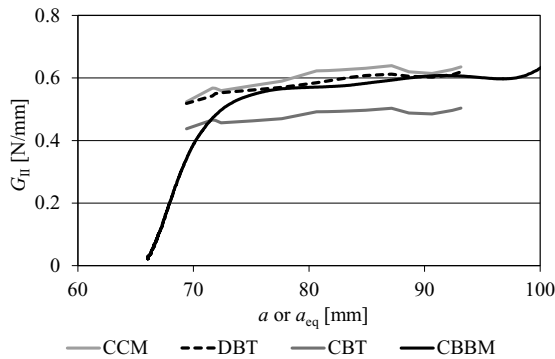


Fig. 4. Representative R -curves for a single test specimen.

The results of Fig. 4 show crack propagation with a steady-state value of G_{II} , thus corresponding to the measurement of G_{IIC} . The CBBM curve is slightly

offset to the right relatively to the other method curves since a_{eq} includes the fracture process zone [12]. In this curve, G_{II} increases up to crack initiation and then it should attain a steady-state value. Between all the methods, the CCM, DBT and CBBM agree quite well, while the CBT predicts smaller values. Table 2 presents the average values and deviation of G_{IIC} (N/mm) of all specimens. As previously discussed in Fig. 4, the CBT under predicts the CBBM (reference) values by 17.7%. This effect was studied in a different work [21], and it was justified by the fact that an offset exists in the compliance vs. a curve between the experiments and numerical simulations, although not changing the curve slope. This could be originated by a slight deviation between the fracture of the correction fluid layer used to track the evolution of a during the test and the real crack tip.

Table 2. Values of G_{IIC} (N/mm) obtained by all methods.

Adhesive	Araldite® AV138			
Specimen	CCM	DBT	CBT	CBBM
1	0.469	0.566	0.440	0.572
2	*	0.709	0.566	0.712
3	*	0.650	0.608	0.724
4	-	-	-	-
5	*	0.578	0.519	0.594
6	0.568	0.579	0.487	0.562
7	0.605	0.581	0.478	0.576
8	0.603	0.583	0.481	0.585
Average	0.561	0.606	0.511	0.618
Deviation	0.064	0.053	0.058	0.069

* Polynomial fitting difficulties

4.2. Inverse technique to obtain the CZM laws

The shear CZM law that best described the adhesive layer for each one specimen was obtained by the inverse fitting technique. For each one of the tests, the CBBM value of G_{IIC} was input in the triangular CZM law and the value of t_s^0 was assessed by fitting the numerical to the experimental P - δ curve. The initial stiffness of the law was directly defined by the adhesive stiffness, while the shear failure displacement was computed internally, knowing that the area under the CZM law is given by G_{IIC} .

Fig. 5 shows a representative example of the final result of the fitting procedure for the Araldite® AV138. During the fitting procedure, the effect of each of the CZM parameters was assessed and resulted as follows: (1) the Young's modulus of the adherends

influences the elastic slope of the curve, (2) G_{IIC} affects the peak value of P by translation of the descending part of the curve (without changing the elastic slope) and (3) t_s^0 slightly increases the peak load and highly affects the specimen stiffness up to the peak load, leading to a more abrupt post-peak load reduction with the increase of t_s^0 [12].

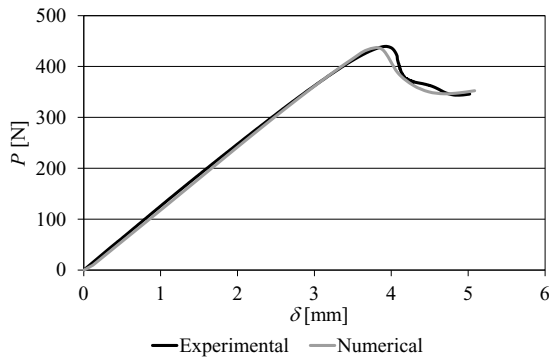


Fig. 5. Example of the fitting procedure for one specimen.

In view of this behaviour, it can be concluded that a unique CZM law exists for each specimen and, as it can be observed in Fig. 5, the triangular CZM managed to capture with accuracy the adhesive layer behaviour. Fig. 6 shows, as example, the full set of CZM laws for the Araldite® AV138 after the fitting procedure.

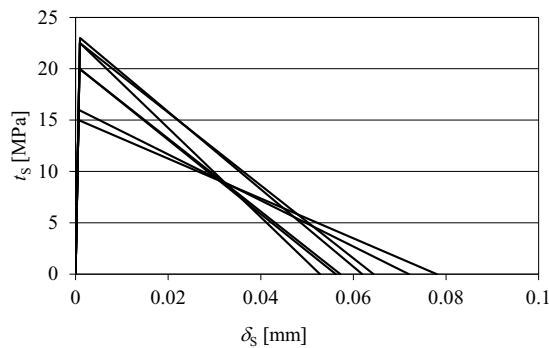


Fig. 6. Set of cohesive laws of the Araldite® AV138.

The average CZM law of the Araldite® AV138 has the following properties: $t_s^0=19.86$ MPa and $G_{IIC}=0.618$ N/mm. The obtained values significantly differ from the data of Table 1, namely $\tau_f=30.2$ MPa and $G_{IIC}=0.38$ N/mm, and this can be justified by using different test methods and specimen geometries. Actually, it is known that the cohesive parameters are highly dependent between bulk and adhesive joint testing, and also on the restraining effects to the

adhesive layer, which varies with the specimens' geometry [12,21].

5. Conclusions

This work enabled the estimation of G_{IIC} of adhesive joints between aluminium adherends and bonded by a brittle adhesive, considering the ENF test geometry. The CCM, DBT, CBT and CBBM were evaluated with this purpose. A fair agreement was found between specimens, which showed the repeatability of the tests. On the other hand, between data reduction methods, the CCM, DBT and CBBM agree well, although in some specimens it was not possible to obtain the CCM prediction because of polynomial fitting difficulties. It was found that the CBT under predicted the values depicted by the other methods by a non-negligible amount (approximately 17%). An explanation of this difference was provided in the paper. The inverse CZM law technique to each individual specimen enabled to accurately reproduce the experimental behaviour of the specimens and to conclude that the triangular CZM law is a good approximation to model the adhesive in shear mode. To conclude, it must be emphasized that full characterization of the adhesives requires both tensile and shear CZM laws, and this is necessary for strength prediction under mixed-mode. With suitable mixed-mode damage initiation and propagation criteria, strength prediction of bonded joints under generic geometric and loading conditions with CZM modelling is enabled.

References

- [1] H. Jin, G.M. Miller, S.J. Pety, A.S. Griffin, D.S. Stradley, D. Roach, N.R. Sottos, S.R. White, *Int. J. Adhes. Adhes.* 44 (2013) 157.
- [2] J. Jumel, M.K. Budzik, N.B. Salem, M.E.R. Shanahan, *Int. J. Solids Struct.* 50 (2013) 297.
- [3] J.D. Barrett, R.O. Foschi, *Eng. Fract. Mech.* 9 (1977) 371.
- [4] K. Leffler, K.S. Alfredsson, U. Stigh, *Int. J. Solids Struct.* 44 (2007) 530.
- [5] M.D. Banea, L.F.M. da Silva, R.D.S.G. Campilho, *J. Adhes.* 88 (2012) 534.
- [6] K.N. Anyfantis, *Eng. Fract. Mech.* 126 (2014) 108.
- [7] R.D.S.G. Campilho, M.D. Banea, F.J.P. Chaves, L.F.M. da Silva, *Comput. Mater. Sci.* 50 (2011) 1543.
- [8] K.C. Pandya, J.G. Williams, *SPE Trans.* 40 (2000) 1765.
- [9] U. Stigh, A. Biel, T. Walander, *Eng. Fract. Mech.* 129 (2014) 67.
- [10] T. Carlberger, U. Stigh, *J. Adhes.* 86 (2010) 816.

- [11] K.S. Alfredsson, A. Biel, S. Salini, *Int. J. Adhes. Adhes.* 62 (2015) 130.
- [12] M.F.S.F. de Moura, R.D.S.G. Campilho, J.P.M. Gonçalves, *Int. J. Solids Struct.* 46 (2009) 1589.
- [13] X. Chen, X. Deng, M.A. Sutton, P. Zavattieri, *Int. J. Mech. Sci.* 79 (2014) 206.
- [14] R.D.S.G. Campilho, M.D. Banea, A.M.G. Pinto, L.F.M. da Silva, A.M.P. de Jesus, *Int. J. Adhes. Adhes.* 31 (2011) 363.
- [15] R.D.S.G. Campilho, M.D. Banea, J.A.B.P. Neto, L.F.M. da Silva, *Int. J. Adhes. Adhes.* 44 (2013) 48.
- [16] M.D. Banea, L.F.M. da Silva, R.D.S.G. Campilho, *J. Adhes.* 91 (2015) 331.
- [17] M.F.S.F. de Moura, A.B. de Morais, *Eng. Fract. Mech.* 75 (2008) 2584.
- [18] R.D.S.G. Campilho, M.F.S.F. de Moura, D.A. Ramantani, J.J.L. Morais, J.J.M.S. Domingues, *Compos. Sci. Technol.* 70 (2010) 371.
- [19] R.D.S.G. Campilho, M.F.S.F. de Moura, A.M.J.P. Barreto, J.J.L. Morais, J.J.M.S. Domingues, *Composites, Part A* 40 (2009) 852.
- [20] M. Ridha, V.B.C. Tan, T.E. Tay, *Compos. Struct.* 93 (2010) 1239.
- [21] M.F.S.F. de Moura, R.D.S.G. Campilho, J.P.M. Gonçalves, *Int. J. Solids Struct.* 46 (2009) 1589.